Carbohydrate Polymer Technologies and Applications 13 (2026) 101096

Contents lists available at ScienceDirect

Carbohydrate Polymer Technologies and Applications

journal homepage: www.sciencedirect.com/journal/carbohydrate-polymer-technologies-and-applications

3D printing of azithromycin loaded gummies for paediatric patients using a carrageenan-based thermoresponsive system

Costanza Fratini [a], Anna Imbriano [b], Ilenia D'Abbrunzo [c], Federica Bigucci [d], Mattia Tiboni [a], Carola Parolin [d], Angela Abruzzo [d], Dritan Hasa [c], Cinzia Pagano [b], Luca Casettari [a,*]

[a] Department of Biomolecular Sciences, School of Pharmacy, University of Urbino Carlo Bo, Via Ca le Suore 2, Urbino, PU 61029, Italy
[b] Department of Pharmaceutical Sciences, University of Perugia, via del Giochetto 6, Edificio B, Perugia 06122, Italy
[c] Department of Chemical and Pharmaceutical Sciences, University of Trieste, Piazzale Europa, 1, Trieste 34127, Italy
[d] Department of Pharmacy and Biotechnology (FaBiT), Alma Mater Studiorum - University of Bologna, Via S. Donato 19/2, Bologna 40127, Italy

ARTICLE INFO

Keywords:
Paediatric compliance
Drug delivery
Solubility enhancement
Emulsion-based formulation
Personalized medicine
Oil-in-water (O/W) emulsion

ABSTRACT

Azithromycin (AZT) is widely used in paediatric medicine, but its poor aqueous solubility and low oral bioavailability (~37 %) limit its therapeutic effectiveness and required high dosages contribute to side effects that reduce treatment adherence. This study presents a formulation strategy that combines solubility enhancement with semisolid extrusion (SSE) 3D printing to produce personalised, chewable AZT-loaded gummies suitable for children.

An oil-in-water (O/W) emulsion was developed using pumpkin seed oil, soy lecithin, and Labrasol® to improve AZT solubility. The emulsion was structured into a printable gel matrix using carrageenan and bentonite nanoclay, enabling extrusion at 62 °C and solidification at 15 °C without post-processing. Rheological analysis confirmed shear-thinning behaviour, high storage modulus, and 85.9 % thixotropic recovery, supporting smooth extrusion and shape retention. Moreover, the printed gummies met European Pharmacopoeia standards for weight and drug content uniformity and remained mechanically stable up to 90 days in packages sealed under vacuum. PXRD confirmed AZT was amorphously dispersed in the developed formulation, and antimicrobial assays showed retained efficacy against *Escherichia coli* and *Staphylococcus aureus*.

This work demonstrates a reproducible and scalable method for paediatric antibiotic delivery that leverages SSE 3D printing, thus offering flexible dosing, improved solubility, and enhanced patient acceptability.

1. Introduction

Azithromycin (AZT), a second-generation macrolide antibiotic, is extensively used in paediatric medicine due to its broad-spectrum Gram-negative and Gram-positive antimicrobial activity, favourable pharmacokinetics, and relatively low incidence of adverse effects (Parnham et al., 2014). It is commonly prescribed for the treatment of respiratory tract, skin and soft tissue infections, and otitis media in children. Its long half-life and tissue penetration allow for short-course therapies (usually around three to five days), which are particularly advantageous in paediatric settings where treatment adherence can be challenging (Bakheit et al., 2014; Wu et al., 2025). Despite its clinical utility, AZT presents several formulation-related challenges that limit its optimal use in children. One of the most significant issues is its poor aqueous solubility, which contributes to low and variable oral bioavailability (approximately 37 %) (Aucamp et al., 2015). AZT is classified as a Biopharmaceutical Classification System (BCS) Class II drug, characterised by low solubility and high permeability. Its large, lipophilic macrolide ring structure and weakly basic nature hinder its dissolution in the acidic environment of the stomach, making its absorption dissolution-rate limited (Bakheit et al., 2014; Luke & Foulds, 1997). This necessitates the use of higher doses to achieve therapeutic plasma concentrations, which can increase the risk of gastrointestinal side effects such as nausea, vomiting, and diarrhoea, common causes of non-adherence in paediatric patients (Dung et al., 2023). To address these challenges, several conventional formulation strategies have been employed, including micronization, solid dispersions, lipid-based systems, and amorphous solid forms (Dung et al., 2023; Lo et al., 2009; Rahman et al., 2024). While these approaches can enhance solubility and bioavailability to some extent, they often fall short in addressing the

* Corresponding author.
E-mail address: luca.casettari@uniurb.it (L. Casettari).

https://doi.org/10.1016/j.carpta.2026.101096

Available online 3 February 2026

broader needs of paediatric patients, such as dose flexibility, palatability, ease of administration, and age-appropriate delivery formats. Currently marketed paediatric formulations of AZT include oral suspensions, dispersible tablets, and granules for reconstitution. These dosage forms are designed to facilitate administration in children who cannot swallow tablets or capsules. However, they are associated with several limitations: fixed dosing restricts personalisation based on weight or age; instability after reconstitution can lead to degradation and reduced efficacy while unpleasant taste can result in poor adherence. Moreover, bulky packaging and the need for precise reconstitution can complicate administration at home or low-resource settings (Thabet et al., 2018).

In recent years, three-dimensional (3D) printing technologies have emerged as a transformative platform in pharmaceutical manufacturing, offering unprecedented opportunities for personalised medicine (Tegegne et al., 2024). Unlike traditional batch manufacturing, 3D printing (3DP) enables the on-demand fabrication of dosage forms with precise control over drug content, shape, release kinetics, and even sensory attributes such as taste and texture (Chen et al., 2020; Vaz & Kumar, 2021). This is particularly relevant in paediatric care, where inter-individual variability in pharmacokinetics and pharmacodynamics necessitates tailored dosing strategies (Rahman et al., 2024). For AZT, 3D printing holds the potential to overcome many of the limitations of current formulations. By enabling the production of chewable dosage forms via specifically tailored formulations, 3D printing can enhance both bioavailability and patient acceptability (Santamaría et al., 2024; Thabet et al., 2018). Importantly, 3D printing also supports the development of age-appropriate formulations that align with the World Health Organization (WHO)'s call for child-friendly medicines (GAP-f & WHO, 2025). This includes the ability to produce low-dose, flexible formulations, as well as visually engaging dosage forms that can improve the medication compliance for young children (Vaz & Kumar, 2021; Veselý et al., 2025). This study aims to investigate an optimised formulation strategy for AZT, considering its physicochemical characteristics and leveraging three-dimensional printing (3DP), specifically the semisolid extrusion (SSE) technique, as a platform for the development of customisable, age-appropriate, and patient-centric dosage forms. To enable 3D printing of AZT into child-friendly dosage forms, an oil-in-water (O/W) emulsion was developed using soy lecithin, Labrasol®, and pumpkin seed oil to enhance drug solubility. Bentonite nanoclay and carrageenan were added to transform the emulsion into a thermoresponsive printable gel matrix. Carrageenan provides reversible gelation properties that support semisolid extrusion and shape retention allowing the formulation to solidify upon cooling without additional curing, making it a key excipient for producing chewable dosage forms via 3DP. By examining the physicochemical challenges of AZT, the limitations of existing formulations, and the capabilities of 3D printing, this work aims to outline a path toward more effective and personalised paediatric antibiotic therapy.

2. Materials and methods

2.1. Materials

Soy lecithin (E322), almond oil, avocado oil and vanilla powder flavour were purchased from A.C.E.F. S.p.A. (Fiorenzuola D'Arda, Italy). Carrageenan E407 (Ceamlacta 2772), from red seaweed of the Rhodophyceae class, break gel strength in milk - Break 2200/3000, gel strength in milk 0,2 % 10 °C - Milk Reactivity 80/110, particle size 98 % gum below 250 μm, it was purchased from Ceamsa. Azithromycin (AZT) dihydrate was supplied by Merck S.p.A. (Milano, Italy). Pumpkin seed oil was purchased from AAkon (Milano, Italy). Labrasol was obtained from Gattefossè SAS (France) while bentonite nanoclay was purchased from Sigma Aldrich (Merck, Germany) and saccharin sodium (E954) from Farmalabor S.r.l. (Italy).

2.2. Solubility studies

AZT dihydrate (250 mg) was dispersed in 5 mL of pumpkin seed oil, almond oil, or avocado oil and stirred at 400 rpm for 24 h at RT. Samples were centrifuged at 4000 rpm for 10 min. The supernatant (3 mL) was transferred into a dialysis bag (Slide-A-Lyzer, Thermo Scientific, Mexico) and immersed in 200 mL EtOH/water (50:50 % v/v) solution. After 72 h, 1.6 mL of dialysate were withdrawn to determine AZT content.

AZT quantification was carried out by UV–Vis spectrophotometry according to the method described by Sultana et al. (2006). Briefly, the dialyzed AZT solution was mixed with HCl 37 % and kept at RT for 90 min in order to induce the AZT degradation. Absorbance was measured at 486 nm using an Agilent 8453 UV-Vis spectrophotometer (Agilent Technologies, Germany). The calibration curve was made in EtOH/-water (50:50 % v/v), $R^2 = 0.99$.

2.3. Oil in water emulsion preparation

An oil in water (O/W) emulsion was prepared as follows: 900 mg of soy lecithin were solubilised in 14.40 g of MilliQ® water (ultrapure Type 1, 18.2 MΩ·cm at 25 °C, TOC $\leq$ 2 ppb) at 60 °C and under magnetic stirring (400 rpm) for 60 min (phase A); 23 mg of AZT dihydrate were solubilised in 2 g of pumpkin seed oil at RT under magnetic stirring (400 rpm) for 60 min (phase B); 428 mg of AZT dihydrate were solubilised in 2.7 g of Labrasol® at RT under magnetic stirring (400 rpm) for 60 min (phase C). Then, maintaining the stirring conditions, phase A was added to phase C and the resulting mixture added to phase B. The so formed emulsion was thus kept at RT under magnetic stirring (400 rpm) overnight. Subsequently, 2.5 g of bentonite were added to the prepared emulsion together with 1.5 g of carrageenan, 200 mg of vanilla powder flavour and 150 mg of saccharin sodium. Then, the mixture underwent high-power ultrasonication (HPU) using a UP200St ultrasonic homogenizer (200 W, 20 kHz; Hielscher Ultrasonics, Germany), 30 % amplitude, for 5 min. The thermal energy generated during the ultrasonication process was utilized to increase the temperature of the system, thereby facilitating the complete dissolution of carrageenan within the formulation.

2.4. Dimensional analysis and zeta potential

The dimensional analysis was performed by Dynamic light scattering (DLS) using a Nicomp 380 ZLS Particle Size (Santa Barbara, California), the same instrument was also used for zeta potential measurement. The sizes were expressed as cumulative volume distributions ($n = 5$) $\pm$ SD. The samples were prepared as follows: 10 μl of the sample were taken from the emulsion and placed in the cuvette, then diluted with ultrapure water. The procedure was repeated until the instrument was able to analyse the sample.

2.5. Rheological properties

Rheological analysis was performed using a MCR 302e rheometer (Anton Paar, Austria) provided with a plate-plate geometry (PP, 25 mm Ø, gap 1 mm), at a controlled temperature of 62 °C thus, mimicking the 3DP conditions. The operating parameters were set as follows. *Flow curve*: shear rate from 0.01 to 10^3 s^{-1}, logarithmic ramp. Shear stress (Pa) and viscosity (Pa*s) were recorded to determine the flow behaviour of the material during the extrusion stage. *Amplitude sweep*: oscillating strain set from 0.001 to 100 %, logarithmic ramp with a fixed angular frequency at 10 rad/s. Storage (G') and loss (G") modulus were recorded and used to determine the linear viscoelastic region (LVR), the yield and flow point (loss of linearity and crossover point, respectively). *3-interval thixotropy test (3ITT) Osc-Osc-Osc:* procedure is shown in Table 1. The percentage of recovery was used to define the thixotropic behaviour of the gels. All the analyses were performed in triplicate.

Table 1
Setting parameters for the *3ITT Osc-Osc-Osc test.*

Step	Oscillating strain (%); angular frequency (rad/s)	Temperature (°C)	Time interval (s)
1	0.01; 10	62, constant	180 s
2	10; 10	62, constant	180 s
3	0.01; 10	62–15, linear ramp at 1 °C/sec	360 s

2.6. 3D-printing of the gummies: CAD design and operating parameters

The most suitable selected formulation was then employed to 3D print AZT-loaded gummies. The selected design (Fig. 1, panel II-A) was obtained using a free Computer-aided Design (CAD) software (Tinkercad®, Autodesk Inc, USA). The 3D printer (BioX, Cellink, Sweden) was equipped with a steel thermoplastic printhead, filled with the pre-formulated gel, and a 0.3 mm nozzle. 3D printing temperature was set at 62 °C and the cartridge left conditioning at that temperature for 15 min prior processing. Bed temperature was instead kept at 15 °C. Infill was set at 80 % with a rectilinear design, pressure around 10–15 kPa and printing speed at 10 mm/s. To enhance adhesion to the printing bed and reduce the moving of the printed structure, a sheet of food grade rubber was added. After preparation the gummies were dried under $CaCl_2$ environment for 24 h. Then, each dried gummy was stored individually in packages under vacuum.

2.7. Gummies characterization

2.7.1. Weight uniformity

The assay was performed, according to the European Pharmacopoeia (Ph. Eur. 11th Ed.), "Uniformity of mass of single-dose preparations" on 20 units of each batch produced. The weight was measured by a calibrated analytical balance (VWR®, Avantor, USA). Results were expressed as mean weight value ± SD.

2.7.2. Drug content and drug content uniformity

For the drug content determination, the 3D-printed gummy was minced by using a scalpel and dispersed in 40 mL of ethanol for 7 days. Then, the suspension was centrifuged at 5000 rpm for 30 min, and the resulting supernatant was filtered through 0.22 μm cellulose nitrate membrane filters (Sartorius AG, Göttingen, Germany) and adequately diluted. Drug concentration in the sample was subsequently measured through HPLC by following the method previously reported (Abruzzo et al., 2022). Briefly, the chromatographic system was composed of a Shimadzu (Milano, Italy) LC-10ATVP chromatographic pump and a Shimadzu SPD-10AVP UV–vis detector. The assay entailed injecting 20 μL samples for analysis using a mobile phase of phosphate buffer (KH_2PO_4 0.01 M adjusted at pH 7.5 with 10 M KOH), methanol and acetonitrile (10/50/40, v/v) through a Phenomenex (Torrance, CA, USA) Kinetex (150 mm × 4.6 mm I.D., 5 μm) column coupled to a Phenomenex (Torrance, CA, USA) Security Guard C18 guard cartridge (4 mm × 3.0 mm I.D., 5 μm). The mobile phase was pumped at a flow rate of 0.8 mL/min, and the eluent was screened at a wavelength of 215 nm. For the drug content uniformity assay, the method reported in the

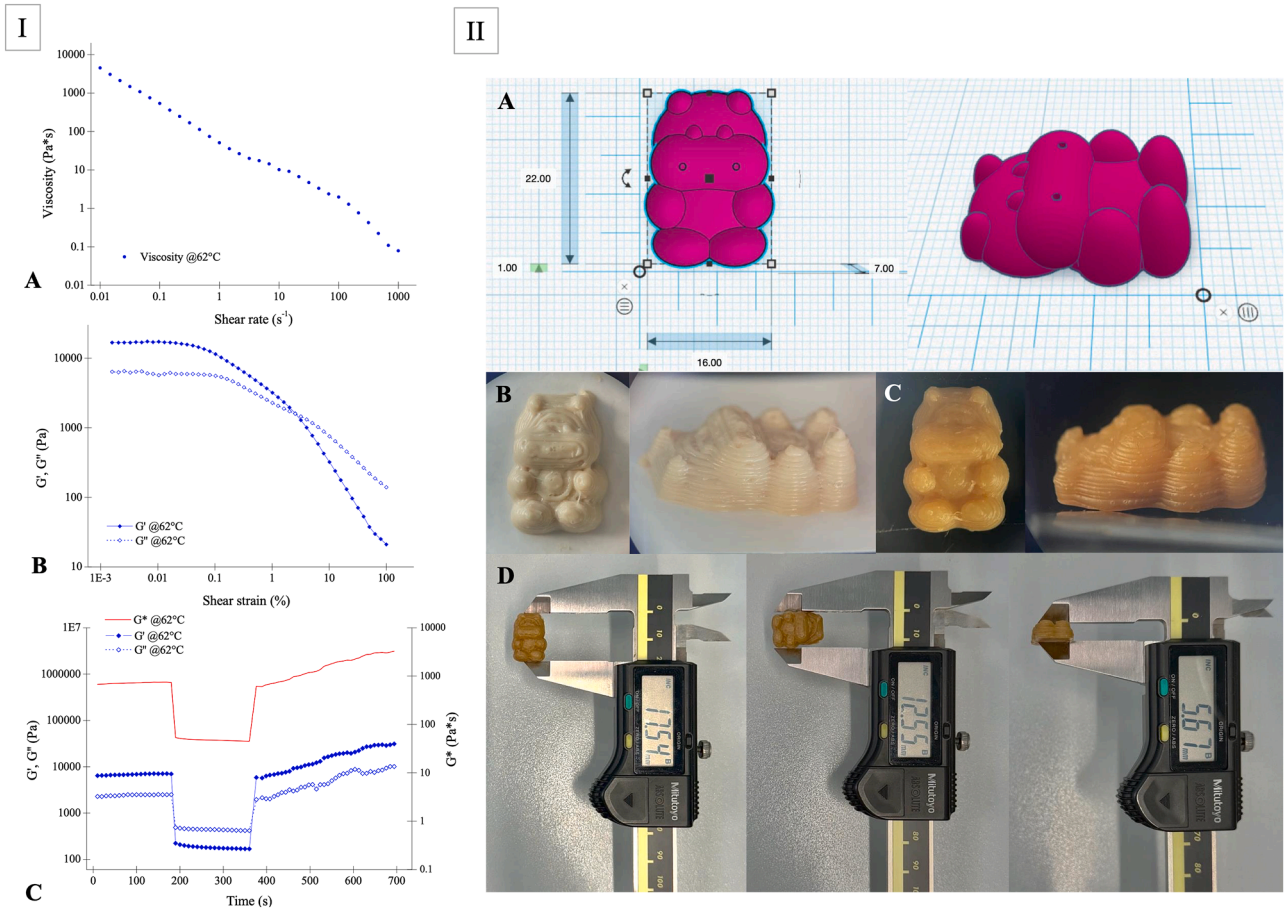

Fig. 1. In panel I are shown the rheological analyses on the AZT-loaded formulation (A) flow curve, (B) amplitude sweep, (C) 3-interval oscillatory test; in panel II are reported computer aided design (CAD) of the gummy showing the set dimensions (A), 3D-printed gummy before (B) and after (C) drying, resulting dimensions of the 3D-printed gummy after 24 h drying (D).

Ph. Eur. 11th Ed. (2.9.6) as "Uniformity of content of single-dose preparations" was followed. Specifically, 10 gummies were randomly taken from each batch produced and analysed to determine the drug amount by using the HPLC.

2.7.3. Texture analysis and stability studies

A texture profile analysis (TPA) was carried out on the 3DP gummies to assess the mechanical properties of the freshly printed formulation (T0) and at subsequent intervals during a 90-day stability study. The samples were stored in individual vacuum-sealed bags at RT (20–25 °C) and protected from light. At each scheduled time point (1, 7, 14, 28, and 90 days), one bag was opened and the gummy was analysed to monitor potential changes in mechanical behaviour. For T5, the analysis was also performed soaking the dosage form in simulated salivary fluid (SSF, composition listed in Table 2) for <60 s. The test was run using a Texture Analyzer, TA.XT plus, (Stable Micro Systems, UK) equipped with a loading cell of 50 Kg and a compression probe (P/20 Ta.Tx, 20 mm diameter). A two-cycle compression was performed. The strain and trigger force were set at 60 % and 5 g, respectively and test speed set at 1 mm/s. 5 s were waited before the second cycle took place. Parameters such as hardness (N), cohesiveness, and gumminess (N) were calculated using Eqs. (1)–(3). Analyses were carried out in triplicate.

$$Hardness(N) = F_1 \quad (1)$$

Where F_1 is the max force registered after the first compression.

$$Cohesiveness = A_2/A_1 \quad (2)$$

Where A_2 and A_1 are the positive areas under the curve of the second and first peak of compression, respectively.

$$Gumminess(N) = Hardness * Cohesiveness \quad (3)$$

Moreover, during the stability studies the average weight and amount of water loss (%) was calculated at each time point using Eq. (4).

$$WL(\%) = [(m_0 - m_x) / m_0] * 100 \quad (4)$$

Where m_0 and m_x are the masses of the dosage form after 24 h drying and at each time point, respectively.

2.7.4. Fourier-transform infrared spectroscopy (FTIR)

The raw materials and AZT-loaded and unloaded 3D-printed gummies were analysed by FTIR (ATR-FTIR, Spectrum Two, Perkin Elmer, USA) to evaluate any possible interaction within the materials and the drug. Transmittance (%) was recorded in the wavelength interval of 4000–400 cm^{-1}. Samples underwent 64 scans using a resolution of 4 cm^{-1}. Air was used as the background for each analysis.

2.7.5. Differential scanning calorimetry (DSC)

The thermal profile of the pure drug, excipients and the 3DP gummies was investigated through DSC (DSC 6000, Perkin Elmer, USA). Specifically, approximately 5 mg of sample were placed in an aluminium pan and heated up from 25 to 250 °C at 10 °C/min. Nitrogen flow rate was kept at 30 mL/min. Analyses were carried out in triplicate.

2.7.6. Powder X-ray diffraction (PXRD) analysis

The 3D-printed gummies, either freshly prepared or aged for 90 days under vacuum packaging, were sectioned into multiple slices for PXRD analysis, and each section was individually mounted on a zero-background silicon sample holder. PXRD patterns were collected using a Bruker D2 Phaser benchtop diffractometer (Bruker, Mannheim, Germany) equipped with Cu Kα radiation ($\lambda = 1.5418$ Å) and a 300 W low-power X-ray generator operating at 30 kV and 10 mA. Data were recorded over a 2θ range of 5–35°, with a step size of 0.02° and a scan rate of 0.6°/s.

Table 2
Simulated salivary fluid (SSF) composition in deionized water, pH = 6.8.

Ingredient	Concentration (mg/L)
Magnesium chloride, anhydrous ($MgCl_2$)	100
Calcium chloride, dihydrate ($CaCl_2$ $2H_2O$)	220
Sodium phosphate dibasic, heptahydrate (Na_2HPO_4 $7H_2O$)	1350
Potassium phosphate monobasic (KH_2PO_4)	680
Potassium chloride (KCl)	750
Urea ($CO(NH)_2$)	600
Sodium chloride (NaCl)	600

2.7.7. In vitro drug release studies

In vitro drug release was carried out to evaluate formulation's ability to release AZT in gastric and intestinal simulated environments. Simulated gastric fluid (SGF) at pH 1.2 was prepared with the following composition: 2 g NaCl, 80 mL HCl 1 M and bidistilled water until 1000 mL. For the intestinal tract, a mixture of simulated intestinal fluid (SIF; KH_2PO_4 0.2 M adjusted at pH 6.8 with KOH 300 g/L) and EtOH (80:20 v/v) was employed to ensure sink conditions. The 3D-printed gummy was cut by a scalpel in fragments to simulate chewing and subsequently placed inside a beaker containing 100 mL of the fluid, thermostated at 37.0 °C ± 0.5 °C. The mixture was stirred with a magnetic stirrer at 100 rpm and at fixed intervals of time (2, 5, 10, 15, 30, 60, 120 min for SGF and 30, 60, 120, 180, 240, 300 and 360 min for SIF) aliquots (1 mL) were withdrawn and immediately replaced with an equal volume of fresh thermostated medium. The same experiment was performed on AZT powder (30 mg) used as control. Aliquots were analyzed immediately after sampling by HPLC-UV method previously described. The experiments were performed in triplicate and results are shown as percentage of cumulative dissolved drug plotted as a function of time.

2.7.8. In vitro antimicrobial activity

The bacterial model strains *Escherichia coli* ATCC 11105 and *Staphylococcus aureus* ATCC 29213 were employed to evaluate the antimicrobial activity of the 3D-printed AZT-loaded gummy. A microdilution assay was carried out to determine Minimal Inhibitory Concentrations (MIC), following NCCLS standard guidelines. Bacterial strains were cultured in Brain Heart Infusion medium (BHI, Difco, Detroit, MI), at 37 °C for 24 h; then 2×10^6 colony forming units (CFU)/mL suspensions were prepared in 2x BHI broth. One gummy was minced with a scalpel and placed in a beaker with 40 mL of water/ethanol mixture 60:40 v/v. After 24 h solutions containing the released drug were withdrawn and analyzed through HPLC-UV. Release solutions containing AZT were subsequently 2-fold serially diluted in sterile water. AZT as pure API dissolved in the same mixture was used as a control. Unloaded 3D-printed gummies and releasing medium (i.e. water/EtOH mixture 60:40 v/v) were also tested following the same procedure and applying the same dilutions. Afterwards, equal amounts of bacterial suspension and diluted free AZT or medium (100 µL each) were put in individual wells of a 96-well plate, reaching AZT concentrations in the range 0.23–30 µg/mL. Plates were incubated at 37 °C for 24 h and then MIC values were determined.

2.8. Statistical analysis

All results are shown as mean ± standard deviation (SD). SD was calculated from the values of three independent experiments. Data from all experiments were analysed using a *t*-test, and differences were considered significant for $p < 0.05$.

3. Results and discussions

3.1. Emulsion composition optimisation

AZT is characterized by low water solubility; thus, the development of a suitable semisolid formulation useful for SSE printing represented a crucial step. To ensure that the drug remained in a molecularly dispersed state, a biphasic system represented by an oil in water (O/W)

nanoemulsion was selected and optimized. A preliminary solubility screening was performed to identify the most suitable oil phase for AZT incorporation. Three vegetable oils namely pumpkin seed oil, almond oil, and avocado oil, were considered. Each oil was selected for its recognized biocompatibility and potential antioxidant contribution, which may further enhance formulation performances. The measured AZT solubility in the selected oils was: 11.85 ± 0.07 mg/mL in pumpkin seed oil, 0.18 ± 0.02 mg/mL in almond oil and 0.17 ± 0.01 mg/mL in avocado oil. Thus, considering that among the tested oils, pumpkin seed oil exhibited the highest solubilizing capacity, it was selected for the nanoemulsion production. This enhanced solubility is likely related to its balanced profile of triglycerides and unsaturated fatty acids, which provides a favourable lipophilic microenvironment for AZT dissolution (Nawirska-Olszańska et al., 2013). In parallel, Labrasol® was selected as the surfactant component due to its well-documented solubilizing and penetration-enhancing properties, which have been shown to improve the oral bioavailability of poorly soluble drugs, including macrolides (Heade et al., 2018; Hu et al., 2001). Soy lecithin was added as a co-surfactant to reinforce interfacial stabilization through its amphiphilic phospholipid structure, thereby improving droplet stability during emulsification and subsequent dispersion (Tabaniag et al., 2023). In combination with Labrasol®, this resulted in a synergistic surfactant system capable of promoting efficient nano-droplet formation and enhancing the overall stability of the emulsion. Specifically, Labrasol® (HLB ≈ 16) was employed as the high-HLB surfactant, useful to improve AZT solubilization and to allow the formation of the O/W system. Soy lecithin (HLB ≈ 7) was used as a co-surfactant to support Labrasol®, reducing the interfacial tension and increasing interfacial film flexibility, thereby improving emulsion stability and preventing phase separation (McClements, 2007). The combined use of surfactants with high-HLB and low-HLB values was considered a valuable strategy to obtain stable nanoemulsions with enhanced drug loading and low polydispersity while limiting the overall surfactant concentration. The nanoemulsion, prepared as reported in methods section, was characterized in terms of particle size, polydispersity index (PDI) and zeta potential. The particle size analysis confirmed the formation of a nanoscale and colloidally stable system, measuring a mean droplet size of 750.90 ± 78.42 nm, a low polydispersity index (PDI = 0.10 ± 0.02), and a negative zeta potential (−29.12 ± 3.59 mV). The narrow size distribution indicates a homogeneous droplet population, while the magnitude of the zeta potential suggests sufficient electrostatic stabilization, contributing to the kinetic stability of the nanoemulsion (McClements, 2007).

As a comparison, to evaluate the enhanced solubilization capacity of the developed nanoemulsion, the same amount of loaded AZT was dispersed in an equivalent volume of bidistilled water (19.15 mL) and stirred at 400 rpm for 24 h at RT. The resulting suspension was then filtered under vacuum and subsequently centrifuged at 4000 rpm for 10 min at RT. AZT concentration in the supernatant was measured by UV analysis obtaining a final concentration of 0.6 mg/mL, which is markedly lower than the concentration achieved in the nanoemulsion (450 mg/19.15 mL).

Following this initial characterization, the nanoemulsion composition was further optimized to improve several critical formulation aspects. The first of these was viscosity: in its original form, the nanoemulsion could not be processed via SSE printing. For this reason, the biopolymer carrageenan was introduced in the external water phase as a rheological modifier. Carrageenan is a polysaccharide extracted from red seaweed of the *Rhodophyceae* class, easily available, non-toxic, cheap, biodegradable and biocompatible and thus suitable for the development of paediatric formulations (J. Liu et al., 2015). It is a linear, sulfated polysaccharide composed of alternating D-galactose and 3, 6-anhydro-D-galactose units linked by α-1,3 and β-1,4 bonds. The main types are classified according to sulfate group content: κ-carrageenan (one sulfate group), ι-carrageenan (two sulfate groups), and λ-carrageenan (three sulfate groups); which determine its gelling, thickening, and stabilizing behavior in formulations. Being a thermosensitive polymer, carrageenan dissolves in water at 70 °C and forms a stable three-dimensional gel network upon cooling, useful for gummies production.

However, carrageenan gel is characterized by poor mechanical properties. To overcome these limitations, bentonite was introduced in the nanocomposition as a reinforcing agent. Bentonite is a lamellar cationic clay, largely used as filler in biopolymer-based systems to enhance their structural properties (Dogaru et al., 2020). Lastly, to enhance the palatability of the formulation, the flavouring agent vanilla powder and the sweetening agent sodium saccharin were added.

3.2. Rheological properties

In the development of semisolid formulations for SSE printing, rheological characterisation is essential to ensure optimal printability and structural integrity (Herrada-Manchón et al., 2023). The rheological behaviour of the formulation governs its flow under applied stress, its ability to be extruded through the nozzle, and its capacity to retain shape upon deposition (Gillispie et al., 2023; Habib & Khoda, 2022). To assess these properties, both shear and oscillatory rheological tests were performed, as illustrated in Fig. 1, panel I.

The formulations demonstrated pronounced shear-thinning behaviour, characterised by a decrease in viscosity with increasing shear rate-an advantageous property for facilitating smooth extrusion (Fig. 1, panel I-A). Oscillatory rheological measurements (Fig. 1, panel I-B) confirmed the predominantly elastic nature of the gel, with the storage modulus (G′) consistently exceeding the loss modulus (G″), indicating solid-like behaviour. Within the linear viscoelastic region (LVR), G′ was measured at approximately 16,387.10 ± 399.37 Pa. A yield point and a crossover were visible at stress values of 4.42 ± 1.09 Pa and 57.77 ± 13.43 Pa, respectively, marking the transition from elastic to viscous behaviour. Additionally, the 3-interval oscillatory (3ITT) test (Fig. 1, panel I-C) demonstrated the thixotropic recovery of the formulation's internal structure following deformation (predominant viscous behaviour, G" > G'), with a recovery of 85.94 %. The 3ITT protocol is specifically designed to evaluate the ability of viscoelastic systems to withstand mechanical stress and subsequently restore their structural integrity once the stress is removed. By alternating between low-strain (undisturbed), high-strain (deformation), and low-strain (recovery) intervals, the test provides insight into the resilience of the material's microstructure and its capacity to recover after shear-induced breakdown (Insua et al., 2025). This property is critical for ensuring printability during extrusion, where temporary structural disruption occurs, and for maintaining stability after deposition, where rapid recovery of the elastic network is required to preserve the intended geometry and mechanical strength of the dosage form (Calafel et al., 2025). Thus, the observed recovery highlights the robustness of the formulation and its suitability for 3D printing applications, where repeated cycles of deformation and recovery are intrinsic to the manufacturing process. Moreover, a temperature-dependent increase in G′, thus in the complex viscosity (G*), was also observed, simulating the thermal gradient experienced during printing—from extrusion at 62 °C to deposition on a cooled print bed at 15 °C. This rheological behaviour can be directly attributed to the presence of carrageenan in the formulation, which is well known to undergo a reversible sol–gel transition depending on temperature. At elevated temperatures, carrageenan exists predominantly in a sol state, facilitating extrusion and flow, whereas upon cooling to near room temperature or below, it reorganizes into a gel network through helix formation and cation-mediated aggregation (S. Liu et al., 2015). This transition underpins the observed increase in elastic modulus and provides structural integrity to the deposited layer enabling the layer-by-layer construction occurring during additive manufacturing. The ability of carrageenan to confer such thermoreversible gelation is therefore critical in ensuring both printability at higher temperatures and mechanical stability at lower temperatures,

highlighting its role as a functional excipient in the design of 3D-printable formulations.

Overall, the rheological profile of the formulation was well-aligned with the requirements for SSE 3D printing, a conclusion further supported by the successful fabrication of 3D-printed gummies exhibiting high shape fidelity and resolution, as detailed in Section 3.3.

3.3. 3D printing of the gummies

The formulation exhibited a temperature-dependent decrease in viscosity, attributed to the presence of carrageenan, a thermo-responsive polymer. Carrageenan completely dissolves at approximately 70 °C and rapidly forms a structured three-dimensional network upon cooling. This thermo-dependent behaviour was leveraged to facilitate extrusion under milder conditions, enabling printing at reduced pressures (~12 kPa). Initial trials revealed that the preliminary formulation possessed insufficient viscosity, resulting in over-extrusion at the lowest operational temperature (50 °C) and pressure (2 kPa). To address this, the polymer concentration was increased to enhance structural integrity during deposition. Through iterative optimisation, the printing parameters were refined to achieve optimal performance: extrusion pressure was set at 12 kPa, nozzle temperature at 62 °C—corresponding to the most favourable viscosity range—and printing speed at 10 mm/s. Fig. 1, panel II-B shows the final 3D-printed gummy. A good shape fidelity and printing resolution were observed and the final dimensions resembled those defined on the CAD design suggesting a good accuracy of the manufacturing process. After 24 h drying under $CaCl_2$ conditions, the gummies were weighed (0.85 ± 0.05 g) and dimensions measured with a digital calliper (Mitutoyo, Japan). The dimensions diminished slightly from 22.00 × 16.00 × 7 mm (width × length × height) (Fig. 1, panel II-A and B) to 17.54 × 12.55 × 5.67 mm (width x length x height) (Fig. 1, panel II-D). Moreover, after drying the gummy appearance was not modified and the structure was maintained as observable in Fig. 1, panel II-B and C.

3.4. 3D-printed gummies characterisation

In recent years, several studies have demonstrated the feasibility of 3D-printed chewable gummies as paediatric-friendly drug delivery systems, highlighting their potential for dose personalization, shape customization, and improved acceptability (Fratini et al., 2025; Holkunde et al., 2025; Imbriano et al., 2025; Laverdière et al., 2025; Santamaría et al., 2024; Stoops et al., 2025). Most of these formulations, however, rely on drugs incorporated in dissolved or dispersed form within hydrophilic polymer matrices. In contrast, the present work introduces a nanoemulsion-based azithromycin system embedded within the gummy matrix, specifically designed to overcome the poor aqueous solubility of this macrolide. By integrating a pre-formed nanoemulsion, the formulation enables more precise control over drug loading, microstructural distribution, and dispersion stability, thereby extending the scope of 3D-printed gummies to the delivery of poorly soluble antibiotics for paediatric therapy.

Following successful fabrication, the printed gummies were comprehensively characterised to verify their quality attributes and to confirm that extrusion-based 3D printing can produce mechanically robust, chewable units with consistent weight, uniform drug content, and suitable textural properties, supporting their use as customizable and flexible paediatric dosage forms.

3.4.1. Weight uniformity

The "Uniformity of mass of single-dose preparations" test outlined in Ph. Eur. 11th Edition (2.9.6) for tablets exceeding 250 mg was adopted. Gummies were weighed immediately after 3D printing to determine the average mass. According to the pharmacopoeia criteria, no more than two individual units per batch may deviate by more than ±5 % from the mean mass. Analysis of the weight distribution, calculated on the weight of each dosage unit straight after printing, (Fig. 2A) revealed that only one or two units per batch fell outside this range. Moreover, the outlier dosages were found to be within the secondary limits ± 10 % thereby confirming compliance with the uniformity requirement. The mean *wet* and *dry* masses were 1.81 ± 0.05 g and 0.85 ± 0.05 g, respectively. The distribution of dry weights (24 h in $CaCl_2$ environment) relative to the mean is also illustrated in Fig. 2B.

3.4.2. Drug content and drug content uniformity

The formulations were designed to contain 30 mg of AZT. Results obtained from the determination of drug content demonstrated that the experimental average amount of AZT was equal to 27.34 ± 0.12 mg per single dose unit. Content uniformity complied with Pharmacopoeia standards (2.9.5, Ph. Eur. 11th Ed.) since the measured content was within the 85–115 % range marked by the general monograph, demonstrating that no drug degradation occurred during printing.

3.4.3. Texture analysis and stability studies

For the evaluation of texture-related mechanical properties, a texture profile analysis (TPA) test was employed to assess parameters such as hardness (N), cohesiveness, and gumminess (N). This method provides insight into the product's ability to withstand a second deformation following an initial compression, thereby offering an indirect metric for evaluating the "chewability" of the 3D-printed gummies (Imbriano et al., 2025). Although a standardised and universally accepted chewability index for gummies is currently lacking, this characteristic remains relevant for determining the ease and comfort of mastication and consumption (Adeleke & Abedin, 2024; Gupta et al., 2015).

Representing the force needed to achieve a specified deformation, hardness measurements were conducted immediately after the drying process (T0), with values slightly exceeding the maximum threshold established by the FDA for chewable tablets (117.68 N) (FDA, 2018). Over the 90-day stability study, hardness remained generally stable for the dosage forms under vacuum packaging, with a notable increase observed at T5. However, upon brief exposure (~30 s) to a minimal volume (1 mL) of simulated salivary fluid (SSF, pH 6.8), a significant reduction in hardness, thus in the resulting gumminess (36.80 ± 6.62 %), was recorded. This suggests that even aged gummies retain sufficient softness for mastication when exposed to saliva for longer periods. Cohesiveness, the amount of force required to overcome internal bonds in the dosage form, instead showed to remain consistent throughout the whole studied period. Results are presented in Table 3 and Fig. 3. Moreover, throughout the 90-days study period, the average weight of the gummies remained largely consistent, with only minimal water loss observed.

3.4.4. Fourier-transform infrared spectroscopy (FTIR)

Attenuated Total Reflectance (ATR)–FTIR spectroscopy was employed to investigate potential chemical interactions among the formulation components and to assess the distribution of AZT within the 3D-printed gummies. Owing to the intrinsic complexity of the formulated matrix, the identification of characteristic AZT absorption bands proved challenging, as spectral overlap hindered the clear resolution of drug-specific peaks. Absorption peaks corresponding to the axial stretching and bending of C–H bonds in methyl groups were observed for AZT in the regions of 2750–3020 cm^{-1} and at 1377 cm^{-1}, respectively. A sharp and intense band at 1719 cm^{-1} was assigned to the axial stretching vibration of the carbonyl (C=O) group within the lactone ring. In addition, significant absorptions were detected in the range of 1134–1221 cm^{-1}, which are consistent with the axial stretching of C–O bonds due to the presence of ether functionalities within the structure (Robaina et al., 2013). Comparative analysis of unloaded and AZT-loaded formulations revealed largely superimposable spectra, with no distinct signals attributable to the API (Fig. 4B). Additionally, each individual excipient was analysed separately (Fig. 4A). The absorption bands and peaks obtained agreed with characteristic ranges described in

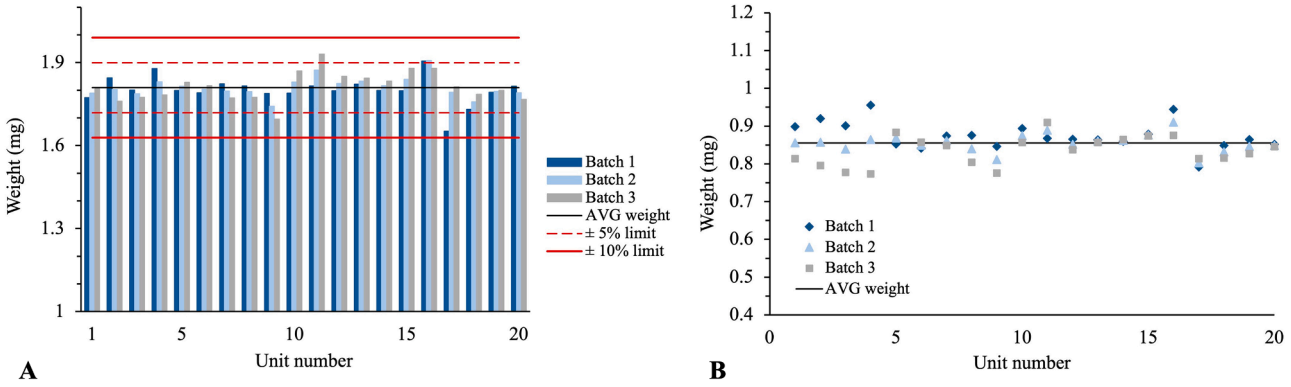

Fig. 2. (A) Distribution of the dosage unit *wet* weights around the average and within the primary and secondary limits (±5 % and ±10 %) given by the Ph. Eur. 11th Ed. for solid oral dosage forms. (B) Distribution of *dry* weights around the average. Each batch comprises 20 units.

Table 3
Mean values ± standard deviation for weight (g), water loss (%), hardness (N), cohesiveness, and gumminess (N) were recorded during a 90-day stability study.

Time point	Days	Weight (g)	WL (%)	Hardness (N)	Cohesiveness	Gumminess (N)
T0	0	0.85 ± 0.05	/	118.88 ± 9.30	0.4 ± 0.03	47.36 ± 6.12
T1	1	0.85 ± 0.04	0.99 ± 0.27	118.98 ± 3.90	0.38 ± 0.01	45.17 ± 0.76
T2	7	0.86 ± 0.07	1.75 ± 0.33	126.08 ± 13.97	0.39 ± 0.03	49.4 ± 9.17
T3	14	0.81 ± 0.07	2.32 ± 0.54	132.83 ± 8.04	0.4 ± 0.01	53.47 ± 4.27
T4	28	0.80 ± 0.07	3.60 ± 0.72	130.7 ± 12.99	0.4 ± 0.05	53.28 ± 10.93
T5	90	0.76 ± 0.02	5.47 ± 0.40	231.59 ± 20.22	0.5 ± 0.04	114.68 ± 11.28
T5@FS	90	/	/	190.17 ± 17.79	0.47 ± 0.01	88.9 ± 7.97

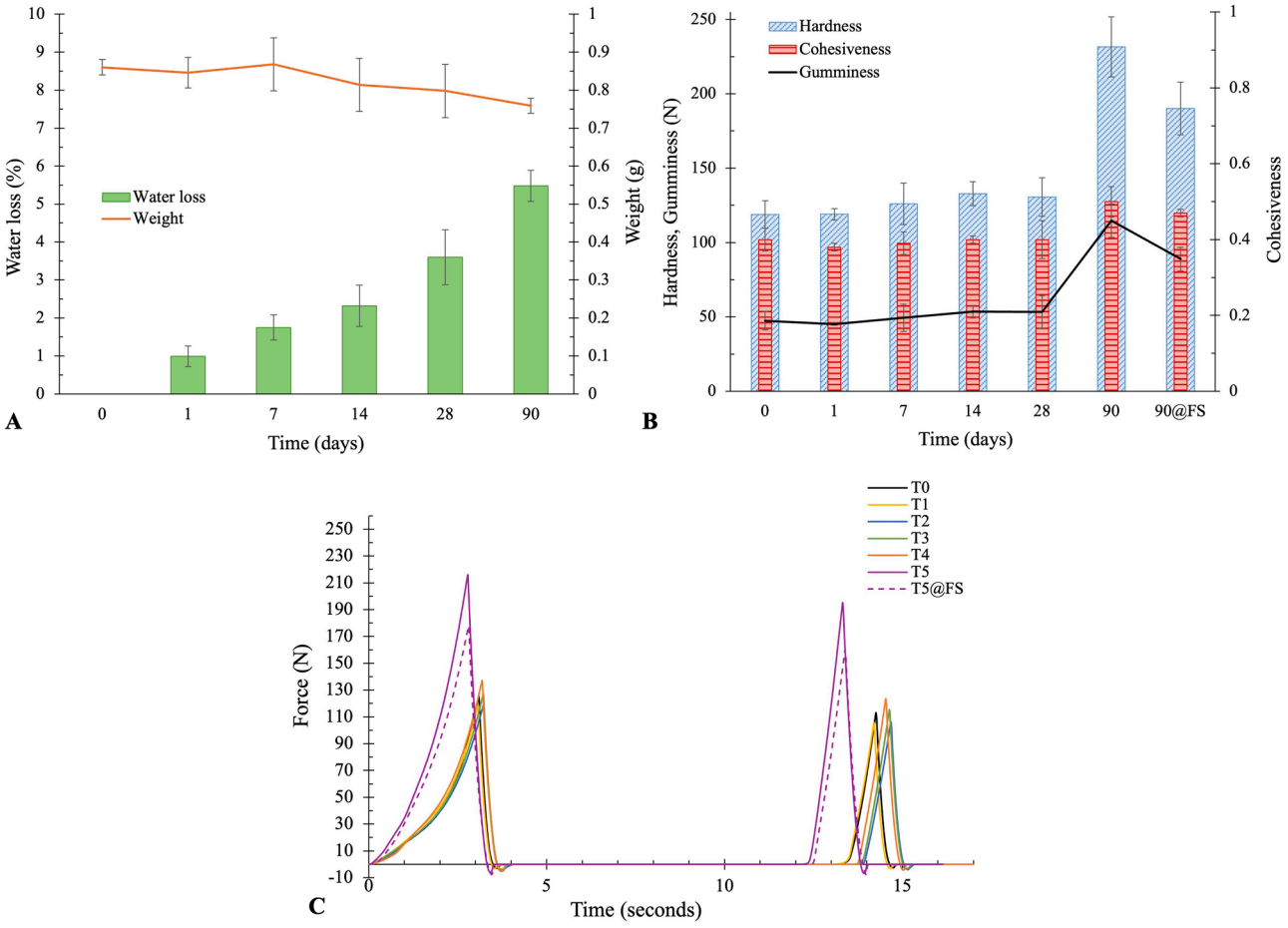

Fig. 3. Mechanical properties of the 3D-printed gummies. (A) average weight (g) and water loss (%); (B) trends of hardness (N), cohesiveness, and gumminess (N); (C) plots of the gummies' texture profile analyses recorded during the 90-days stability study.

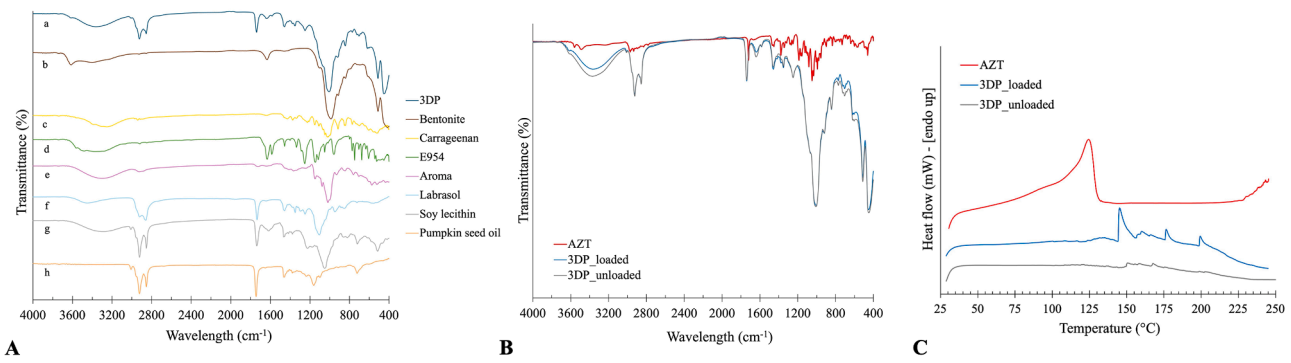

Fig. 4. (A) FTIR spectra of AZT (a), 3D-printed gummy (b), bentonite nanoclay (c), carrageenan (d), saccharin sodium (e), vanilla aroma (f), Labrasol® (g), soy lecithin (h), pumpkin seed oil (i); (B) normalized and overlapped spectra of AZT, unloaded and loaded 3D-printed gummies, showing a close-up to no identification of representative peaks of AZT in the dosage form; (C) DSC thermograms of (bottom-top order): 3D-printed unloaded gummy, 3D-printed loaded gummy, AZT.

the literature and referable to the main peaks identified in the developed formulation, showing no appreciable variations.

3.4.5. *Differential scanning calorimetry (DSC)*

DSC analyses were carried out to evaluate the crystalline state of AZT in the developed formulation. Thermograms of the pure drug and both unloaded and loaded 3D-printed gummies were recorded as illustrated in Fig. 4C. For AZT, dihydrate form, the desorption and evaporation of water were progressive starting at 58.18 °C until one singular endothermic peak that was recorded at 124.42 °C corresponding to the melting of the dehydrated crystals as previously studied (Bondi et al., 2025; D'Abbrunzo et al., 2025). During the analysis of the final 3D-printed dosages (both unloaded and loaded with the API), it was not possible to unambiguously determine the crystalline state of AZT, as degradation of thermolabile excipients started to occur at approximately 95 °C. This degradation interfered with the detection of potential melting or recrystallization transitions of the API, thereby limiting the interpretability of the DSC thermogram with respect to its solid-state characteristics.

3.4.6. *PXRD analysis*

The PXRD pattern of the pure commercial AZT confirms the high crystallinity of the starting material, showing perfect correspondence with the calculated pattern of the dihydrate structure deposited in the Cambridge Structural Database (CSD) (refcode GEGJAD02) (Neglur et al., 2018). No diffraction peaks were detected in any of the five sections of the 3D-printed gummy, indicating that AZT is homogeneously solubilised within the polymeric matrix (Fig. 5A). To evaluate the physical stability of the formulation over time, PXRD analysis was also performed on a 3D-printed gummy stored for 90 days at RT in single package under vacuum. The diffraction data collected from the aged sample confirmed that AZT retained the same amorphous solubilised state as in the freshly prepared formulation, with no evidence of recrystallisation or solid-state transformation (Fig. 5B)

3.4.7. *In vitro drug release studies*

Fig. 6A shows that, the maximum percentage of dissolved AZT in SGF reached 56.15 ± 1.26 % of the total weighed amount after 10 min. This result can be attributed to the degradation of the drug occurring at acidic pH in agreement with previous findings (Assi et al., 2020).After this time point, AZT rapidly degraded and only 38.20 ± 0.41 % was measured after 30 min, time that corresponds to the mean gastric residence time in children (Guimarães et al., 2022).

In contrast, when the 3D-printed gummy was tested, AZT was not detectable in the medium, likely due to the limited partitioning of the drug from the formulation into the SGF combined with its concurrent degradation. To better understand this outcome, an additional experiment was performed in the presence of the 3D-printed gummy. After 30

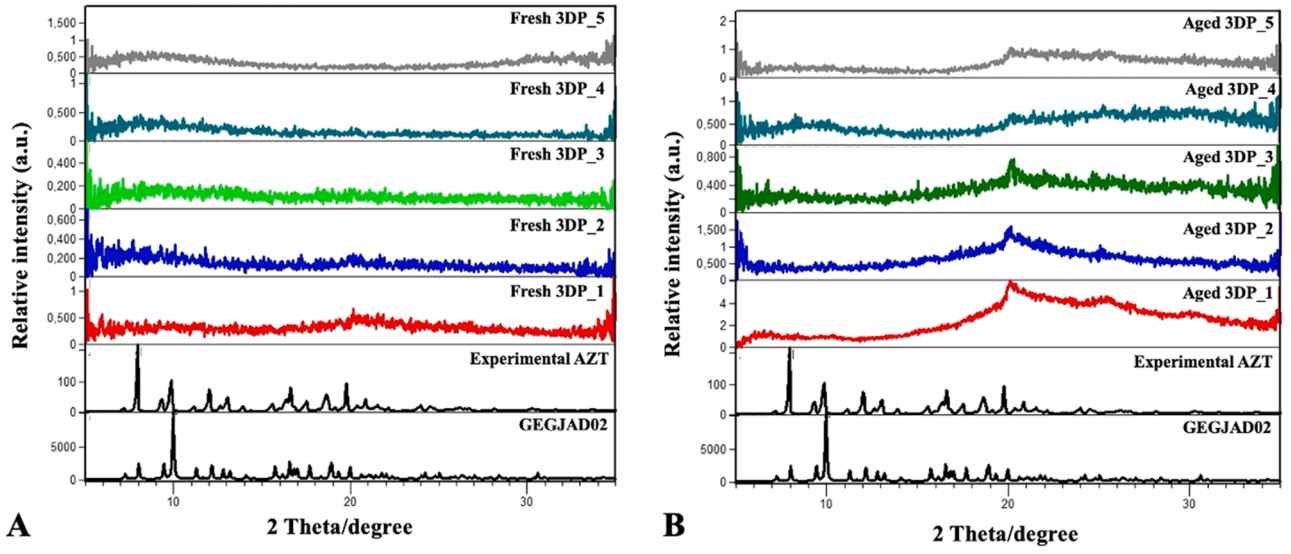

Fig. 5. (A) From bottom to top: PXRD patterns of the CSD-deposited structure (GEGJAD02), pure commercial AZT, and five different sections of a freshly prepared 3D-printed gummy. (B) From bottom to top) PXRD patterns of the CSD-deposited structure (GEGJAD02), pure commercial AZT, and five different sections of a 90-day aged 3D-printed gummy.

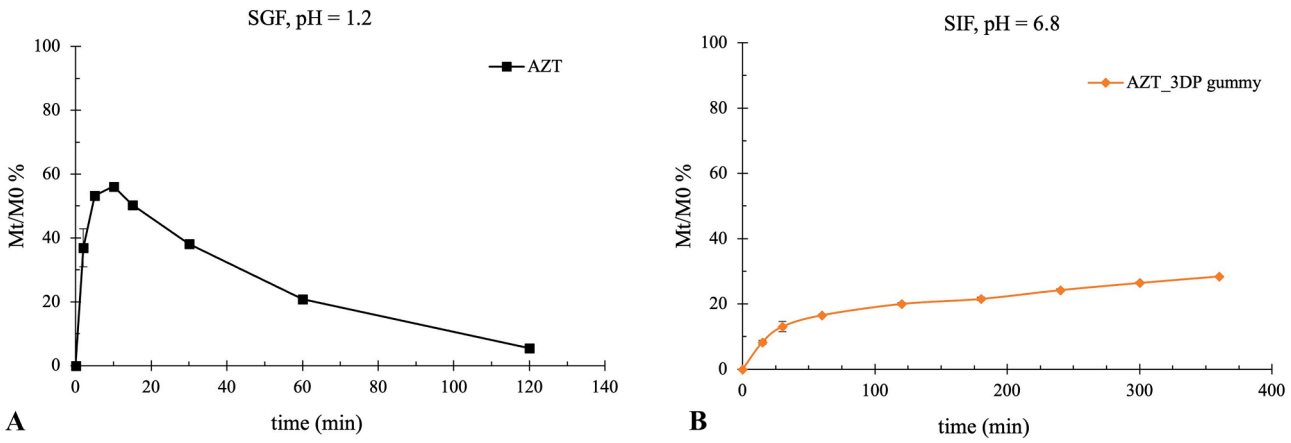

Fig. 6. Dissolution profiles of (A) AZT pure drug in simulated gastric fluid (SGF, pH = 1.2) and (B) AZT-loaded 3D-printed gummies in simulated intestinal fluid (SIF, pH = 6.8).

min, the SGF was removed, and the pellet obtained from the fragmented gummy was isolated, resuspended in ethanol (50 mL), and stirred (200 rpm) for 96 h to quantify the amount of drug retained within the formulation. HPLC analysis revealed that 79.2 ± 4.1 % of the drug remained inside the gummy. This finding is particularly relevant, as it demonstrates that the 3D-printed formulation can protect AZT from acidic degradation and may therefore enable higher drug concentrations to reach the intestinal tract compared to AZT alone. As a matter of fact, regarding the *in vitro* release in SIF, a sustained AZT release profile was observed in the presence of the 3D-printed gummy (Fig. 6B), likely due to the low drug partitioning from the formulation, as previously discussed. Although these results provide only a preliminary indication of the formulation's behaviour in the intestinal environment, the prolonged release of AZT may be advantageous for the treatment of infections (Yus et al., 2020), such as respiratory bacterial infections, for which AZT remains one of the most commonly prescribed antibiotics in paediatrics patients.

3.4.8. *In vitro antimicrobial activity*

The antimicrobial activity of AZT loaded gummies was tested towards two model strains, *S. aureus* ATCC 29213 and *E. coli* ATCC 11105, by microdilution assay. MIC values of free AZT were 1 μg/mL for both microbial strains, in accordance with the literature (Bondi et al., 2025; Lugli et al., 2025) and it remained unchanged for AZT delivered by the 3D-printed gummies. These data indicate that AZT retained the antimicrobial effect when included in the developed formulation. Moreover, unloaded formulation and releasing medium alone (i.e. water/ethanol mixture 60:40 v/v) did not interfere with microbial growth at the dilutions corresponding to AZT MIC. These samples inhibited bacterial growth at dilutions equivalent to 7.5 μg/mL and higher. Consequently, the antimicrobial activity observed at lower concentrations (1 μg/mL AZT) can be attributed exclusively to the effect of AZT.

4. Conclusion

This study provides a formulation and manufacturing approach for producing paediatric-friendly azithromycin (AZT) dosage forms using semisolid extrusion (SSE) 3D printing. By combining an oil-in-water (O/W) emulsion with a thermoresponsive gel matrix composed of carrageenan and bentonite nanoclay, a printable system capable of generating chewable gummies with consistent weight, drug content, and mechanical properties was developed. The formulation showed rheological behaviour suitable for extrusion, including shear-thinning flow and high thixotropic recovery, which enabled accurate deposition and shape retention. The printed gummies complied with European Pharmacopoeia standards and remained physically stable over 90 days. PXRD confirmed that AZT was amorphously dispersed within the matrix, with no recrystallisation observed during storage time. Additionally, antimicrobial testing demonstrated that the drug in the final formulation retained its activity against *Escherichia coli* and *Staphylococcus aureus* after printing. This work highlights the potential of combining solubility-enhancing emulsions with SSE 3D printing to produce personalised, age-appropriate antibiotic formulations that address key limitations of existing paediatric products, including poor solubility, fixed dosing, and low acceptability.

Funding

This study is part of the project "3D-printed antibiotic oral dosage forms for paediatric use" [p3Diatrics] under the Project of Relevant National Interest (PRIN 2022) call, funded by Ministero dell'Università e della Ricerca. Project ID: 2022FRNFMT

CRediT authorship contribution statement

Costanza Fratini: Writing – original draft, Investigation, Formal analysis, Data curation. **Anna Imbriano:** Investigation, Formal analysis, Data curation. **Ilenia D'Abbrunzo:** Writing – original draft, Formal analysis, Data curation. **Federica Bigucci:** Writing – review & editing, Conceptualization. **Mattia Tiboni:** Methodology, Investigation. **Carola Parolin:** Writing – original draft, Investigation, Formal analysis, Data curation. **Angela Abruzzo:** Writing – original draft, Methodology, Investigation, Funding acquisition, Conceptualization. **Dritan Hasa:** Writing – review & editing, Funding acquisition, Conceptualization. **Cinzia Pagano:** Writing – review & editing, Funding acquisition, Conceptualization. **Luca Casettari:** Writing – review & editing, Project administration, Funding acquisition, Conceptualization.

Declaration of competing interest

The authors declare that they have no known competing financial interests or personal relationships that could have appeared to influence the work reported in this paper.

The author is an Editorial Board Member/Editor-in-Chief/Associate Editor/Guest Editor for this journal and was not involved in the editorial review or the decision to publish this article.

Acknowledgments

The authors gratefully acknowledge Ilaria Marinelli for the technical assistance and support provided during the experimental work.

Data availability

Data will be made available on request.

References

Abruzzo, A., Parolin, C., Rossi, M., Vitali, B., Cappadone, C., & Bigucci, F. (2022). Development and characterization of azithromycin-loaded microemulsions: A promising tool for the treatment of bacterial skin infections. *Antibiotics, 11*(8). https://doi.org/10.3390/antibiotics11081040

Adeleke, O. A., & Abedin, S. (2024). Characterization of prototype gummy formulations provides insight into setting quality standards. *AAPS PharmSciTech, 25*(6). https://doi.org/10.1208/s12249-024-02876-w

Assi, R. A., Abdulbaqi, I. M., Ming, T. S., Yee, C. S., Wahab, H. A., Asif, S. M., & Darwis, Y. (2020). Liquid and solid self-emulsifying drug delivery systems (Sedds) as carriers for the oral delivery of azithromycin: Optimization, *in vitro* characterization and stability assessment. *Pharmaceutics, 12*(11), 1–29. https://doi.org/10.3390/pharmaceutics12111052

Aucamp, M., Odendaal, R., Liebenberg, W., & Hamman, J. (2015). Amorphous azithromycin with improved aqueous solubility and intestinal membrane permeability. *Drug Development and Industrial Pharmacy, 41*(7), 1100–1108. https://doi.org/10.3109/03639045.2014.931967

Bakheit, A. H. H., Al-Hadiya, B. M. H., & Abd-Elgalil, A. A. (2014). Azithromycin. In *Profiles of drug substances, excipients and related methodology, 39* pp. 1–40). Academic Press Inc. https://doi.org/10.1016/B978-0-12-800173-8.00001-5

Bondi, G., D'Abbrunzo, I., Hasa, D., Parolin, C., Vitali, B., Bertoni, S., Imbriano, A., Pagano, C., Fratini, C., Sabbatini, B., Bigucci, F., & Abruzzo, A. (2025). Innovative bilayered buccal films: A paediatric-friendly dosage form for transmucosal azithromycin delivery. *International Journal of Pharmaceutics, 684*. https://doi.org/10.1016/j.ijpharm.2025.126164

Calafel, M. I., Criado-Gonzalez, M., Aguirresarobe, R., Fernández, M., & Mijangos, C. (2025). From rheological concepts to additive manufacturing assessment of hydrogel-based materials for advanced bioprinting applications. In *Materials advances, 6* pp. 4566–4597). Royal Society of Chemistry. https://doi.org/10.1039/d5ma00019j

Chen, G., Xu, Y., Kwok, P. C. L., & Kang, L. (2020). Pharmaceutical applications of 3D printing. In *Additive manufacturing, 34*. Elsevier B.V.. https://doi.org/10.1016/j.addma.2020.101209

D'Abbrunzo, I., Battaiotto, L., Abruzzo, A., Bondi, G., Bigucci, F., Pagano, C., Imbriano, A., Fratini, C., Casettari, L., Voinovich, D., & Hasa, D. (2025). Structural insights into novel coamorphous systems of azithromycin with faster dissolution profile. *European Journal of Pharmaceutics and Biopharmaceutics, 216*. https://doi.org/10.1016/j.ejpb.2025.114873

Dogaru, B. I., Simionescu, B., & Popescu, M. C. (2020). Synthesis and characterization of κ-carrageenan bio-nanocomposite films reinforced with bentonite nanoclay. *International Journal of Biological Macromolecules, 154*, 9–17. https://doi.org/10.1016/j.ijbiomac.2020.03.088

Dung, P. T. P., Trinh, T. D., Nguyen, Q. H., Nguyen, H. M., Nguyen, N. C., Tran, N. B., Tran, C. S., Nguyen, T. H. N., & Tung, N. T. (2023). Development of taste-masking microcapsules containing azithromycin by fluid bed coating for powder for suspension and *in vivo* evaluation. *Journal of Microencapsulation, 40*(5), 345–356. https://doi.org/10.1080/02652048.2023.2209639

FDA. (2018). Quality attribute considerations for chewable tablets guidance for industry. http://www.fda.gov/Drugs/GuidanceComplianceRegulatoryInformation/Guidances/default.htm.

Fratini, C., Aluigi, A., Tiboni, M., & Casettari, L. (2025). 3D-printed chewable gummies: A customizable approach to formulate propranolol in the paediatric population. *Journal of Drug Delivery Science and Technology, 114*. https://doi.org/10.1016/j.jddst.2025.107581

GAP-f, & WHO. (2025). Transforming the paediatric medicines ecosystem. https://www.who.int/publications/i/item/9789240110632.

Gillispie, G. J., Copus, J., Uzun-Per, M., Yoo, J. J., Atala, A., Niazi, M. K. K., & Lee, S. J. (2023). The correlation between rheological properties and extrusion-based printability in bioink artifact quantification. *Materials and Design, 233*. https://doi.org/10.1016/j.matdes.2023.112237

Guimarães, M., Somville, P., Vertzoni, M., & Fotaki, N. (2022). Performance evaluation of montelukast pediatric formulations: Part I—Age-related *in vitro* conditions. *AAPS Journal, 24*(1). https://doi.org/10.1208/s12248-021-00661-2

Gupta, A., Chidambaram, N., & Khan, M. A. (2015). An index for evaluating difficulty of chewing index for chewable tablets. *Drug Development and Industrial Pharmacy, 41*(2), 239–243. https://doi.org/10.3109/03639045.2013.858736

Habib, M. A., & Khoda, B. (2022). Rheological analysis of bio-ink for 3D bio-printing processes. *Journal of Manufacturing Processes, 76*, 708–718. https://doi.org/10.1016/j.jmapro.2022.02.048

Heade, J., Maher, S., Bleiel, S. B., & Brayden, D. J. (2018). Labrasol ® and salts of medium-chain fatty acids can Be combined in low concentrations to increase the permeability of a macromolecule marker across isolated rat intestinal mucosae. *Journal of Pharmaceutical Sciences, 107*(6), 1648–1655. https://doi.org/10.1016/j.xphs.2018.02.012

Herrada-Manchón, H., Fernández, M. A., & Aguilar, E. (2023). Essential guide to hydrogel rheology in extrusion 3D printing: How to measure it and why it matters?. In *Gels, 9* Multidisciplinary Digital Publishing Institute (MDPI). https://doi.org/10.3390/gels9070517

Holkunde, A., Karnik, I., Uttreja, P., Narala, N., Wang, H., Elkanayati, R. M., Vemula, S. K., & Repka, M. A. (2025). Personalized medicine through Semisolid-extrusion based 3D printing: Dual-drug loaded gummies for enhanced patient compliance. *Pharmaceutical Research, 42*(1), 185–201. https://doi.org/10.1007/s11095-024-03813-z

Hu, Z., Tawa, R., Konishi, T., Shibata, N., & Takada, K. (2001). A novel emulsifier, Labrasol, enhances gastrointestinal absorption of gentamicin. *Life Sciences, 69*. https://doi.org/10.1016/s0024-3205(01)01375-3

Imbriano, A., Fratini, C., Bondi, G., D'Abbrunzo, I., Bertoni, S., Tiboni, M., Abruzzo, A., Hasa, D., Pagano, C., & Casettari, L. (2025). 3D-printed chewable gummy tablets: A new tool for oral amoxicillin administration in paediatric population. *International Journal of Pharmaceutics, 677*. https://doi.org/10.1016/j.ijpharm.2025.125645

Insua, I., Etzold, O., Calafel, I., Aguirresarobe, R., Calderón, M., & Fernández, M. (2025). Rheological insight into the 3D printability of carboxymethyl cellulose-based hydrogels. *Gels, 11*(4). https://doi.org/10.3390/gels11040259

Laverdière, J., Bendicho-Lavilla, C., Mahrouche, L., Friciu, M., Pastore, Y., Leclair, G., Basit, A. W., Goyanes, A., & Roullin, V. G. (2025). 3D printed hydroxyurea for pediatric use: Toward personalized formulations and reduced exposure risk. *International Journal of Pharmaceutics*, 686. https://doi.org/10.1016/j.ijpharm.2025.126326

Liu, J., Zhan, X., Wan, J., Wang, Y., & Wang, C. (2015). Review for carrageenan-based pharmaceutical biomaterials: Favourable physical features versus adverse biological effects. In *Carbohydrate polymers, 121* pp. 27–36). Elsevier Ltd. https://doi.org/10.1016/j.carbpol.2014.11.063

Liu, S., Chan, W. L., & Li, L. (2015). Rheological properties and scaling laws of κ-carrageenan in aqueous solution. *Macromolecules, 48*(20), 7649–7657. https://doi.org/10.1021/acs.macromol.5b01922

Lo, J. B., Appel, L. E., Herbig, S. M., McCray, S. B., & Thombre, A. G. (2009). Formulation design and pharmaceutical development of a novel controlled release form of azithromycin for single-dose therapy. *Drug Development and Industrial Pharmacy, 35*(12), 1522–1529. https://doi.org/10.3109/03639040903037223

Lugli, S., Abruzzo, A., Parolin, C., Vitali, B., Bolognesi, M. L., Brucale, M., Valle, F., Cerchiara, T., Luppi, B., & Bigucci, F. (2025). Mucoadhesive polymer-coated liposomes as a promising approach to counteract bacteria responsible for aerobic vaginitis. *International Journal of Pharmaceutics, 677*. https://doi.org/10.1016/j.ijpharm.2025.125667

Luke, D. R., & Foulds, G. (1997). Disposition of oral azithromycin in humans. *Clinical Pharmacology and Therapeutics, 61*(6), 641–648. https://doi.org/10.1016/S0009-9236(97)90098-9

McClements, D. J. (2007). Critical review of techniques and methodologies for characterization of emulsion stability. *Critical Reviews in Food Science and Nutrition, 47*(7), 611–649. https://doi.org/10.1080/10408390701289292

Nawirska-Olszańska, A., Kita, A., Biesiada, A., Sokół-Łętowska, A., & Kucharska, A. Z. (2013). Characteristics of antioxidant activity and composition of pumpkin seed oils in 12 cultivars. *Food Chemistry, 139*(1–4), 155–161. https://doi.org/10.1016/j.foodchem.2013.02.009

Neglur, R., Hosten, E., Aucamp, M., Liebenberg, W., & Grooff, D. (2018). Water and the relationship to the crystal structure stability of azithromycin: Thermal investigations of solvatomorphism, amorphism and polymorphism. *Journal of Thermal Analysis and Calorimetry, 132*(1), 373–384. https://doi.org/10.1007/s10973-017-6928-6

Parnham, M. J., Haber, V. E., Giamarellos-Bourboulis, E. J., Perletti, G., Verleden, G. M., & Vos, R. (2014). Azithromycin: Mechanisms of action and their relevance for clinical applications. In *Pharmacology and therapeutics, 143* pp. 225–245). Elsevier Inc. https://doi.org/10.1016/j.pharmthera.2014.03.003

Rahman, A. U., Khan, M., Khan, M. A., Rehman, M. U., Abdullah, & Ahmed, S. (2024). Pharmacokinetics and histotoxic profile of a novel azithromycin-loaded lipid-based nanoformulation. *AAPS PharmSciTech, 25*(6). https://doi.org/10.1208/s12249-024-02861-3

Robaina, N. F., de Paula, C. E. R., Brum, D. M., de la Guardia, M., Garrigues, S., & Cassella, R. J. (2013). Novel approach for the determination of azithromycin in pharmaceutical formulations by Fourier transform infrared spectroscopy in film-through transmission mode. *Microchemical Journal, 110*, 301–307. https://doi.org/10.1016/j.microc.2013.04.015

Santamaría, K. J., Anaya, B. J., Lalatsa, A., González-Barranco, P., Cantú-Cárdenas, L., & Serrano, D. R. (2024). Engineering 3D printed gummies loaded with metformin for paediatric use. *Gels, 10*(10). https://doi.org/10.3390/gels10100620

Stoops, M., Do, B., Ramos, S., Tan, B. X., Sheng Chua, N. Y., Mazet, R., Guiblin, N., Michelet, A., Flynn, S., Abbou, S., Goyanes, A., Rieutord, A., Legrand, F. X., & Annereau, M. (2025). Clinical implementation of a paediatric 3D-printed combination of sulfamethoxazole and trimethoprim. *International Journal of Pharmaceutics*, 676. https://doi.org/10.1016/j.ijpharm.2025.125581

Sultana, N., Arayne, M. S., Hussain, F., & Fatima, A. (2006). Degradation studies of azithromycin and its spectrophotometric determination in pharmaceutical dosage forms. *Pakistan Journal of Pharmaceutical Sciences, 19*(2), 98–103.

Tabaniag, J. S. U., Abad, M. Q. D., Morcelos, C. J. R., Geraldino, G. V. B., Alvarado, J. L. M., & Lopez, E. C. R. (2023). Stabilization of oil/water emulsions using soybean lecithin as a biobased surfactant for enhanced oil recovery. *Journal of Engineering and Applied Science, 70*(1). https://doi.org/10.1186/s44147-023-00322-5

Tegegne, A. M., Ayenew, K. D., & Selam, M. N. (2024). Review on recent advance of 3DP-based pediatric drug formulations. In *BioMed research international, 2024*. Hindawi Limited. https://doi.org/10.1155/2024/4875984

Thabet, Y., Klingmann, V., & Breitkreutz, J. (2018). Drug formulations: Standards and novel strategies for drug administration in pediatrics. *Journal of Clinical Pharmacology, 58*, S26–S35. https://doi.org/10.1002/jcph.1138

Vaz, V. M., & Kumar, L. (2021). 3D Printing as a promising tool in personalized medicine. In *AAPS pharmscitech, 22*. Springer Science and Business Media Deutschland GmbH. https://doi.org/10.1208/s12249-020-01905-8

Veselý, M., Záruba, D., & Elbl, J. (2025). Development of 3D-printed chewable gummy tablets with adjustable ondansetron content for the treatment of pediatric patients. *Pharmaceutics, 17*(4). https://doi.org/10.3390/pharmaceutics17040458

Wu, K., Wu, S., & Wang, L. (2025). The impact of azithromycin on lung function in children and adolescents with cystic fibrosis: A systematic review and meta-analysis. In *Clinical therapeutics, 47* pp. 918–924). Elsevier Inc. https://doi.org/10.1016/j.clinthera.2025.07.008

Yus, C., Irusta, S., Sebastian, V., & Arruebo, M. (2020). Controlling particle size and release kinetics in the sustained delivery of oral antibiotics using pH-independent mucoadhesive polymers. *Molecular Pharmaceutics, 17*(9), 3314–3327. https://doi.org/10.1021/acs.molpharmaceut.0c00408